ELSEVIER

Journal of Fluids and Structures 20 (2005) 1073–1084

JOURNAL OF FLUIDS AND STRUCTURES

www.elsevier.com/locate/jfs

Transient analysis of dam–reservoir interaction including the reservoir bottom effects

S. Küçükarslan[a,*], S.B. Coşkun[b], B. Taşkın[c]

[a]*Civil Engineering Department, Celal Bayar University, PK 44, Manisa 45000, Turkey*
[b]*Civil Engineering Department, Niğde University, Niğde, Turkey*
[c]*Civil Engineering Department, İstanbul Technical University, Maslak,34469, İstanbul, Turkey*

Received 8 October 2003; accepted 12 May 2005

Abstract

In this paper, time-domain transient analysis of elastic dam–reservoir interaction including the reservoir bottom effects is presented by coupling the finite element method in the infinite fluid domain and in the solid domain. An efficient coupling procedure is formulated by a substructuring method. Sommerfeld's boundary condition for the far end of the infinite domain is implemented. To verify the proposed scheme, numerical examples are given to compare with available exact solutions for rigid and elastic dam cases. Finally, a numerical example is studied to evaluate the effects of the reservoir bottom.

Keywords: Dam–reservoir interaction; Finite element method; Transient response of dam; Reservoir bottom absorption

1. Introduction

A dam–reservoir system subjected to a strong earthquake is likely to behave nonlinearly, even though the concrete material of the dam remains elastic. Therefore, a transient analysis of the structure interacting with a fluid and subjected to the earthquake ground motion is necessary for a realistic analysis. Westergaard (1933) initially originated the estimation of the hydrodynamic pressures on the concrete dams. By assuming the water to be incompressible, Zangar and Haefei (1952) and Zienkiewicz and Nath (1963) determined the hydrodynamic pressures on the dams experimentally, establishing an analogy between the electric potential problem and the dam interaction problem. Chopra (1968) reported that the effect of water compressibility is significant for seismic response. Later, Saini et al. (1978), Chopra and Chakrabarti (1981), Hall and Chopra (1982), Fenves and Chopra (1985) and Lotfi et al. (1987), studied this problem in the frequency domain by using the finite element method. Finite element time-domain analyses were done by Sharan (1987) and Tsai et al. (1990). In time-domain formulations, researchers used a radiation boundary condition for the far end or for the near end to take into account the radiating waves. A radiation boundary condition at the far end of a finite reservoir introduces damping in the system and models the loss of energy by the outgoing waves. Analytical solutions for the far boundary were performed by Chwang and Hausner (1978) and Liu (1986).

*Corresponding author. Tel.: +90 546 2364993; fax: +90 236 2412143.
E-mail address: semih.kucukarslan@bayar.edu.tr (S. Küçükarslan).

0889-9746/$ - see front matter © 2005 Elsevier Ltd. All rights reserved.
doi:10.1016/j.jfluidstructs.2005.05.004

Another method, which was used by Kuo (1982), is the added mass approach. In this method, the linear and nonlinear responses of the dam–reservoir interaction are approximated by the addition of a number of masses into the dam equation.

For linear analysis, the frequency-domain formulations are simpler, but for a nonlinear analysis of the structure it is necessary to develop time-domain formulations. The added mass type of formulation can be used for both the linear and nonlinear analyses but it is not appropriate for cracked dams under earthquake loads (Ghaemian and Ghobarah, 1998). The finite element method was used to discretize the fluid domain and the far end was modelled by using the radiation boundary conditions of Sharan (1987) or Sommerfeld (1949). These two radiation boundary conditions are the simplest; more complicated boundary conditions were developed as in Tsai et al. (1990), Maity and Bhattacharyya (1999) and Li et al. (1996). The complicated boundary condition for the far end gives better results even when the radiating boundary is located very near to the dam surface, but its implementation in a finite element code is tedious. Mostly, the simplest boundary conditions are preferred in the analyses, but due to the approximation made in the transmitting boundary, it is necessary to use a sufficiently large numbers of elements.

A parametric study on the fluid–structure interaction problem was realized by Maity and Bhattacharyya (2003), recently. In their study, an iterative scheme in the dynamic analysis and a complicated boundary condition was used. However, in this study, a direct time integration with a simple radiating boundary condition is considered in the dynamic analysis of dam–reservoir interaction. Finally, a simple and 1-D model is implemented to take into account the effects of the sediments for the bottom absorption effects.

2. Analytical formulation

Fig. 1. illustrates the geometry of a dam–reservoir system. In the formulation of the dam–reservoir interaction, a substructure method is used. The uncoupled structural and fluid responses are presented separately. The coupling is done via the interfaces that take into account the interaction forces between the dam and reservoir.

2.1. Structural responses

The solid dam is discretized by using finite elements, and the equations of the system subjected to the ground motion including the effects of reservoir are written as

$$[M]\{\ddot{u}\} + [C]\{\dot{u}\} + [K]\{u\} = -[M]\{\ddot{u}_g\} + \{E(t)\}, \tag{1}$$

where $[M]$ is the mass matrix, $[C]$ is the structural damping matrix, $[K]$ is the structural stiffness matrix, $\{u\}$ is the vector of nodal displacements relative to the ground, $\{\ddot{u}_g\}$is the vector of ground accelerations, $\{E(t)\}$is the vector of nodal point forces associated with the hydrodynamic pressures produced by the reservoir; the over-dot defines the differentiation with respect to time.

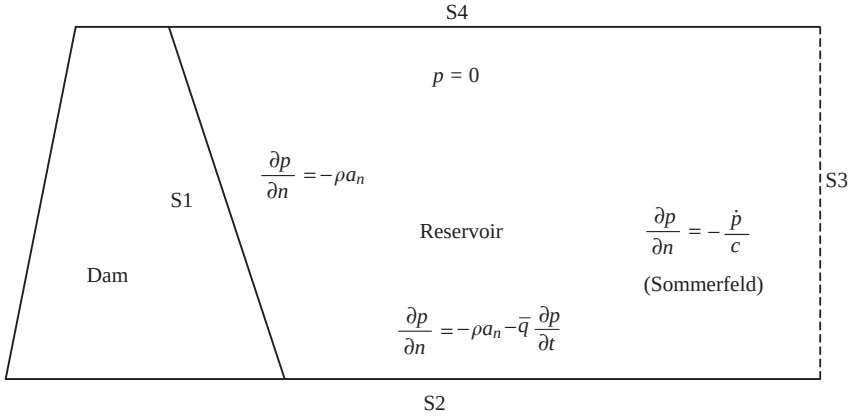

Fig. 1. Dam and reservoir.

The structural damping in the system is included by using a Rayleigh type of damping matrix,

$$[C] = b_1[M] + b_2[K], \tag{2}$$

where b_1 and b_2 are variable factors to obtain a desirable damping in the system.

2.2. Reservoir responses

For a compressible inviscid fluid, the hydrodynamic pressure p resulting from ground motion of the rigid dam (Fig. 1) satisfies the wave equation,

$$\nabla^2 p = \frac{1}{c^2}\frac{\partial^2 p}{\partial t^2}, \tag{3}$$

where c is the velocity of the sound in water and ∇^2 is the Laplacian operator in two dimensions.

The following boundary conditions are defined by assuming the effects of surface waves and viscosity of the fluid are neglected.

(i) *At the fluid–solid interface* (S1):

$$\frac{\partial p}{\partial n} = -\rho a_n, \tag{4}$$

where a_n is the normal acceleration on the interface and ρ is mass density of the fluid.

(ii) *At the bottom of the fluid domain* (S2):

$$\frac{\partial p}{\partial n} = -\rho a_n - \bar{q}\frac{\partial p}{\partial t}, \tag{5a}$$

where $\bar{q}$ is a damping coefficient which is the fundamental parameter characterizing the effects of the reservoir bottom materials and it is given in Fenves and Chopra (1984) as

$$\bar{q} = \frac{1-\alpha_b}{c(1+\alpha_b)}, \tag{5b}$$

in which α_b is the ratio of the amplitude of the reflected hydrodynamic pressure wave to the amplitude of a vertically propagating pressure wave incident on the reservoir bottom.

The absorption of the pressure waves at the reservoir bottom is an important factor that may significantly affect the magnitude of the hydrodynamic force on the dam. Fenves and Chopra (1984) investigated the effects of sedimentary material deposited on the reservoir bottom. As well as employing an approximate boundary condition to simulate energy absorption into the sediment, they suggested that the sediment can play a significant role in modulating the response of the concrete gravity dams. Lotfi and Tassoulas (1986) modelled the sediment as a linearly viscoelastic, nearly incompressible solid. The analysis was based on the finite element method and used hyperelements in which all interactions were taken into account. Medina and Dominguez (1989) carried out calculations using the boundary element method and obtained results similar to those of Lotfi and Tassoulas (1986). Cheng (1986) investigated the effects of poroelastic sediment on the hydrodynamic force on a rigid dam, seated on a half-plane viscoelastic foundation. Bougacha and Tassoulas (1991) modelled the sediment material as a poroelastic continuum. The rigorous poroelastic model for the sediment material requires accurate information on the layer characteristics, such as material grain size, porosity, degree of saturation and hydraulic conductivity. These details are not readily available for the existing structures. Besides, from a computational point of view, this approach requires an enormous amount of computation. Therefore, a simple boundary condition, Eq. (5a), is used in the work of Yang et al. (1996) and in the current work.

(iii) *At the far end* (S3): A Sommerfeld-type radiation boundary condition can be implemented, namely

$$\frac{\partial p}{\partial n} = -\frac{\dot{p}}{c}. \tag{6}$$

(iv) At the free surface (S4),

$$p = 0. \tag{7}$$

Eqs. (3)–(7) can be discretized using finite elements to give a matrix equation of the form

$$[G]\{\ddot{p}\} + [H]\{p\} = \{B\}, \tag{8}$$

where

$$H_{ij} = \sum \int_{R_e} \left[\frac{\partial N_i}{\partial x}\frac{\partial N_j}{\partial x} + \frac{\partial N_i}{\partial y}\frac{\partial N_j}{\partial y} \right] \mathrm{d}R, \tag{9}$$

$$G_{ij} = \sum \frac{1}{c^2} \int_{R_e} N_i N_j \, \mathrm{d}R, \tag{10}$$

$$B_i = \sum \int_{S_e} N_i \frac{\partial p}{\partial n} \, \mathrm{d}S. \tag{11}$$

In Eqs. (9)–(11), N_i defines the shape function, R_e and S_e denote the region and external boundary of an element, respectively.

If Eq. (8) is partitioned and appropriate boundary conditions, Eqs. (4)–(7), are substituted in Eq. (11), one can write

$$\begin{bmatrix} G_{11} & G_{12} & G_{13} & G_{14} \\ G_{21} & G_{22} & G_{23} & G_{24} \\ G_{31} & G_{32} & G_{33} & G_{34} \\ G_{41} & G_{42} & G_{43} & G_{44} \end{bmatrix} \begin{Bmatrix} \ddot{p}_1 \\ \ddot{p}_2 \\ \ddot{p}_3 \\ \ddot{p}_4 \end{Bmatrix} + \begin{bmatrix} H_{11} & H_{12} & H_{13} & H_{14} \\ H_{21} & H_{22} & H_{23} & H_{24} \\ H_{31} & H_{32} & H_{33} & H_{34} \\ H_{41} & H_{42} & H_{43} & H_{44} \end{bmatrix} \begin{Bmatrix} p_1 \\ p_2 \\ p_3 \\ p_4 \end{Bmatrix} = \begin{Bmatrix} B_1 \\ B_2 \\ B_3 \\ 0 \end{Bmatrix}, \tag{12}$$

in which

$$B_1 = \int_{S1} N_1 q_1 \, \mathrm{d}S, \quad B_2 = \int_{S2} N_2 q_2 \, \mathrm{d}S, \quad B_3 = \int_{S3} N_3 q_3 \, \mathrm{d}S, \tag{12a}$$

where subscripts '1', '2', '3' and '4' represent the dam–reservoir interface, the dam–foundation interface, the far truncating end, and the free surface, respectively. q_1 is equal to $-\rho(\ddot{u}_s + \ddot{u}_g)$, in which ρ is the mass density of the fluid, $\ddot{u}_s$ is the nodal acceleration produced by the flexible dam, and q_2 and q_3 are equal to $(-\rho\ddot{u}_g - \bar{q}\dot{p}_2)$ and $-\dot{p}_3/c$, respectively.

Rewriting Eq. (12), results in the following form:

$$[G]\{\ddot{p}\} + [C_f]\{\dot{p}\} + [H]\{p\} = \{b\}, \tag{13}$$

in which

$$[C_f] = \begin{bmatrix} 0 & 0 & 0 & 0 \\ 0 & \bar{q} & 0 & 0 \\ 0 & 0 & 1/c & 0 \\ 0 & 0 & 0 & 0 \end{bmatrix}, \tag{14}$$

$$\{b\}^{\mathrm{T}} = \{-\rho S^{\mathrm{T}}(\ddot{u}_s + \ddot{u}_g) \quad -\rho S^{\mathrm{T}}\ddot{u}_g \quad 0 \quad 0\}, \tag{15}$$

where $S = \int N_i^{\mathrm{T}} N_j \, \mathrm{d}S$.

3. Coupling of the dam and reservoir equations

The substructuring technique is used to couple the finite elements of the discretized dam domain and the reservoir domain by applying the pressure and displacement boundary conditions on the common interfaces, i.e. on the surface S1 (Fig. 1).

Applying the Newmark method to Eq. (1) yields

$$[\bar{K}]\{u^i\} = \{R^i\}, \tag{16}$$

in which the superscript 'i' represents the ith time step,

$$[\bar{K}] = [K] + a_0[M] + a_1[C], \tag{17}$$

$$\{R^i\} = -[M]\{\ddot{u}_g\} + \{E^i\} + [M](a_0\{u^{i-1}\} + a_2\{\dot{u}^{i-1}\} + a_3\{\ddot{u}^{i-1}\}) + [C](a_1\{u^{i-1}\} + a_4\{\dot{u}^{i-1}\} + a_5\{\ddot{u}^{i-1}\}), \tag{18}$$

where

$$a_0 = \frac{1}{\beta\Delta t^2}, \quad a_1 = \frac{\gamma}{\beta\Delta t}, \quad a_2 = \frac{1}{\beta\Delta t}, \quad a_3 = \frac{1}{2\beta} - 1, \quad a_4 = \frac{\gamma}{\beta} - 1, \quad a_5 = \frac{\Delta t}{2}\left(\frac{\gamma}{\beta} - 2\right). \tag{19}$$

For the given values of $\gamma = 0.5$ and $\beta = 0.5$, the suggested method is unconditionally stable. By applying the Newmark method to Eq. (13), one can detain the following:

$$[\bar{H}]\{p^i\} = \{b^i\}, \tag{20}$$

in which

$$[\bar{H}] = [H] + a_0[G] + a_1[C_f], \tag{21}$$

$$\{b^i\} = \begin{Bmatrix} -\rho S^{\mathrm{T}}(\ddot{u}_s^i + \ddot{u}_g^i) \\ -\rho S^{\mathrm{T}}\ddot{u}_g^i \\ 0 \\ 0 \end{Bmatrix} + [G](a_0\{p^{i-1}\} + a_2\{\dot{p}^{i-1}\} + a_3\{\ddot{p}^{i-1}\}) + [C_f](a_1\{p^{i-1}\} + a_4\{\dot{p}^{i-1}\} + a_5\{\ddot{p}^{i-1}\}), \tag{22}$$

where $\ddot{u}_s^i$ is the nodal acceleration on the dam–reservoir interface and it is given by

$$\{\ddot{u}_s^i\} = a_0(\{u_s^i\} - \{u_s^{i-1}\}) - a_2\{\dot{u}_s^{i-1}\} - a_3\{\ddot{u}_s^{i-1}\}. \tag{23}$$

By substituting Eq. (23) into Eq. (22) and rewriting Eq. (22), one can obtain

$$\begin{aligned} \{b^i\} = {} & \begin{Bmatrix} -\rho S^{\mathrm{T}}[a_0(\{u_s^i\} - \{u_s^{i-1}\}) - a_2\{\dot{u}_s^{i-1}\} - a_3\{\ddot{u}_s^{i-1}\} + \ddot{u}_g^i] \\ -\rho S^{\mathrm{T}}\ddot{u}_g^i \\ 0 \\ 0 \end{Bmatrix} \\ & + [G](a_0\{p^{i-1}\} + a_2\{\dot{p}^{i-1}\} + a_3\{\ddot{p}^{i-1}\}) \\ & + [C_f](a_1\{p^{i-1}\} + a_4\{\dot{p}^{i-1}\} + a_5\{\ddot{p}^{i-1}\}). \end{aligned} \tag{24}$$

Let

$$[h] = [\bar{H}]^{-1} = \begin{bmatrix} h_1 \\ h_2 \\ h_3 \\ h_4 \end{bmatrix} = \begin{bmatrix} h_{11} & h_{12} & h_{13} & h_{14} \\ h_{21} & h_{22} & h_{23} & h_{24} \\ h_{31} & h_{32} & h_{33} & h_{34} \\ h_{41} & h_{42} & h_{43} & h_{44} \end{bmatrix}. \tag{25}$$

In a 3-D analysis, the computational efficiency of the solution considerably decreases by taking the inverse of the $[\bar{H}]$ matrix. By substituting Eq. (25) in Eq. (20), one obtains

$$\{p^i\} = [h]\{b^i\}. \tag{26}$$

Since the pressures on surface S1 of the dam are contributed to the structural equation as $\{E(t)\}$, one can write the ith step in the following form:

$$\{E^i\} = [S]\{p_1^i\}, \tag{27}$$

where $[S]$ is a transformation matrix which transforms the pressures to the nodal forces for a given surface. By rewriting Eq. (16), one obtains

$$[\hat{K}]\{u^i\} = \{\hat{R}^i\}, \tag{28}$$

where

$$[\hat{K}] = [K] + a_0([M] + [\bar{M}]) + a_1[C], \tag{29}$$

$$\begin{aligned} \{\hat{R}^i\} = {} & -([M] + [\bar{M}])\{\ddot{u}_g\} + ([M] + [\bar{M}])(a_0\{u^{i-1}\} + a_2\{\dot{u}^{i-1}\} + a_3\{\ddot{u}^{i-1}\}) + [C](a_1\{u^{i-1}\} + a_4\{\dot{u}^{i-1}\} \\ & + a_5\{\ddot{u}^{i-1}\}) - \{E^*\}, \end{aligned} \tag{30}$$

$$[\bar{M}] = \begin{bmatrix} 0 & 0 & 0 & 0 \\ 0 & 0 & 0 & 0 \\ 0 & 0 & 0 & 0 \\ 0 & 0 & 0 & \bar{M}_{S1} \end{bmatrix}, \tag{31}$$

$$\{E^*\} = \begin{Bmatrix} 0 \\ 0 \\ 0 \\ E^*_{S1} \end{Bmatrix}, \tag{32}$$

$$[\bar{M}_{S1}] = \rho[S][h_{11}][S^{\mathrm{T}}], \tag{33}$$

$$\{E^*_{S1}\} = [S][h_1][G](a_0\{p^{i-1}\} + a_2\{\dot{p}^{i-1}\} + a_3\{\ddot{p}^{i-1}\}) + [S][h_1][C_f](a_1\{p^{i-1}\} + a_4\{\dot{p}^{i-1}\} + a_5\{\ddot{p}^{i-1}\}) + \rho[S][h_{12}][S^{\mathrm{T}}](\ddot{u}^i_g). \tag{34}$$

Eq. (28) is the final form of the equations for obtaining the ith step values of the displacements and the corresponding velocities and accelerations as follows:

$$\{\dot{u}^i\} = \{\dot{u}^{i-1}\} + a_6\{\ddot{u}^{i-1}\} + a_7\{\ddot{u}^i\}, \tag{35}$$

$$\{\ddot{u}^i\} = a_0(\{u^i\} - \{u^{i-1}\}) - a_2\{\dot{u}^{i-1}\} - a_3\{\ddot{u}^{i-1}\}, \tag{36}$$

where $a_6 = \Delta t(1-\gamma)$ and $a7 = \gamma\Delta t$.

By substituting the values of the calculated ith step displacements in Eq. (28) to values in (24), the ith step pressures for the fluid domain can be calculated in Eq. (26). The first and the second derivatives of the pressure can be calculated similarly to Eqs. (35) and (36) as

$$\{\dot{p}^i\} = \{\dot{p}^{i-1}\} + a_6\{\ddot{p}^{i-1}\} + a_7\{\ddot{p}^i\}, \tag{37}$$

$$\{\ddot{p}^i\} = a_0(\{p^i\} - \{p^{i-1}\}) - a_2\{\dot{p}^{i-1}\} - a_3\{\ddot{p}^{i-1}\}. \tag{38}$$

This ends the coupling process for the ith step; then, the next time steps need to be calculated by applying the same procedure.

4. Numerical examples

First, a rigid dam (Fig. 2) with a constant reservoir height 180 m extending to infinity under a ramp acceleration (Fig. 3) is studied by using finite elements; then, an elastic dam (Fig. 2) analysis is carried out. Finally, the effect of bottom absorption is investigated. In all analyses, the wave speed c used is 1439 m/s and the water is assumed to be compressible and inviscid with a mass density of $\rho = 1000\,\mathrm{kg/m^3}$.

4.1. Vertical rigid dam

In the finite element method, linear 4-noded serendipity (rectangular) elements are chosen. In the horizontal direction 40 elements and in the vertical direction 20 elements are used. The hydrodynamic pressure at the bottom of the reservoir is plotted in Fig. 4 and compared with the exact solution (Tsai et al., 1990) (for $x = 0$),

$$p(x,z,t) = \frac{-2\rho c}{H_f}\left\{\sum_{k=1}^{\infty}\frac{(-1)^k\cos(\lambda_k z)}{\lambda_k}\int_0^{t-x/c} a_n \mathrm{J}_0\left(\lambda_k c\sqrt{(t-\tau)^2 - \frac{x^2}{c^2}}\right)\mathrm{d}\tau\right\} \tag{39}$$

where $\lambda_k = (2k-1)\pi/2H_f$, H_f is the height of the fluid and J_0 is the Bessel function of first kind; a_n is the ramp acceleration shown in Fig. 3.

The distribution of the hydrodynamic pressure on the solid surface, when the hydrodynamic pressure reaches the peak value at the bottom, is plotted in Fig. 5. In all of the figures, the dimensionless hydrodynamic pressure is

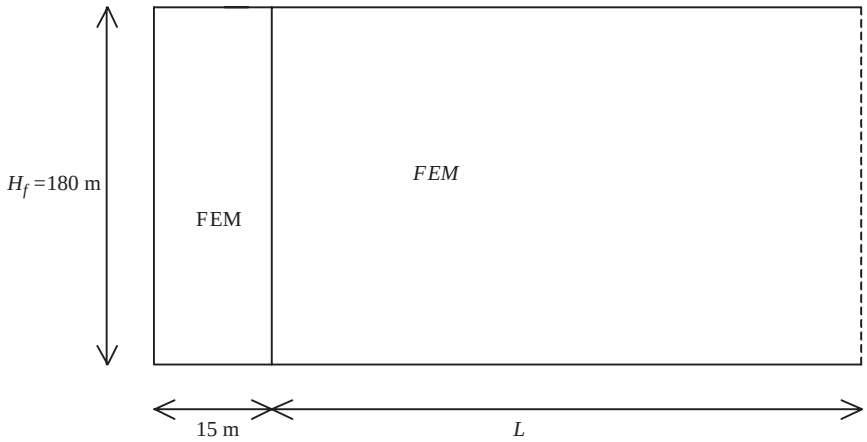

Fig. 2. Vertically faced dam.

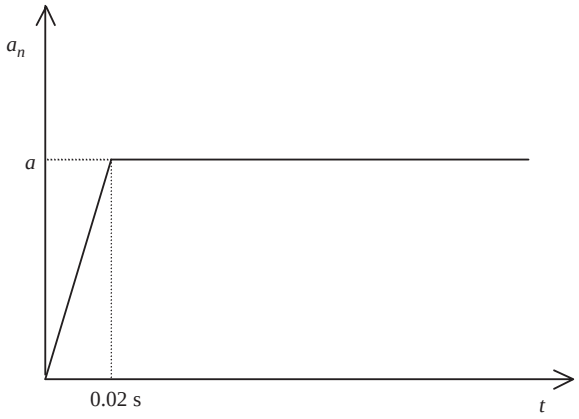

Fig. 3. Ramp acceleration.

defined as

$$\frac{p}{aH_f\rho}, \tag{40}$$

where a is the maximum value of the ramp acceleration.

4.2. Vertical flexible dam

A reservoir of height 180 m, constant along the length of the dam (extending to "infinity") and a width of 15 m (Fig. 2) is analyzed under earthquake ground acceleration (Fig. 6). The dam has an elasticity modulus of 3.43×10^{11} N/m^2, Poisson's ratio of 0.0, and mass density of 2400 kg/m^3. FEM–FEM coupling is performed with linear 4-noded rectangular elements. For the dam, three elements in the horizontal direction and 12 elements in the vertical direction are used. For the reservoir, 30 elements in the horizontal direction and 12 elements in the vertical direction are used. The far end is truncated at a distance of 900 m and Sommerfeld's boundary condition is implemented for the radiating waves. Analyses are performed considering a time step of 0.01 s. Results are successfully compared with the available exact solutions of Lee and Tsai (1991) and Tsai and Lee (1991), and plotted for the bottom pressure distribution of the dam as seen in Fig. 7 and for the displacements at the top point of the structure as in Fig. 8. In Figs. 6–8, g is the acceleration due to gravity.

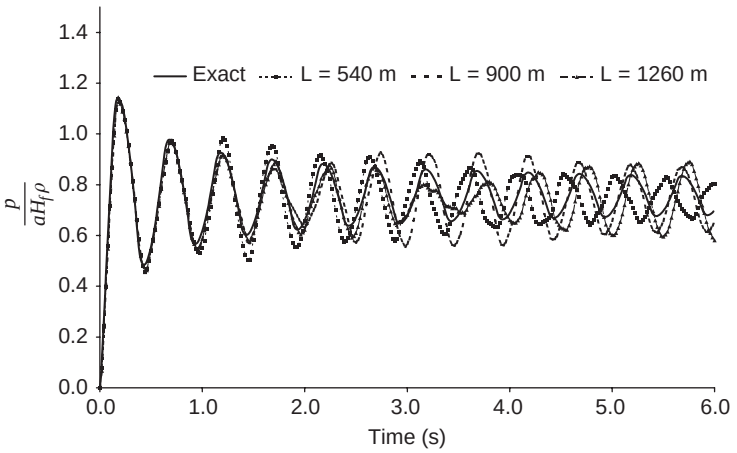

Fig. 4. Comparison of the hydrodynamic pressure at the bottom of the dam.

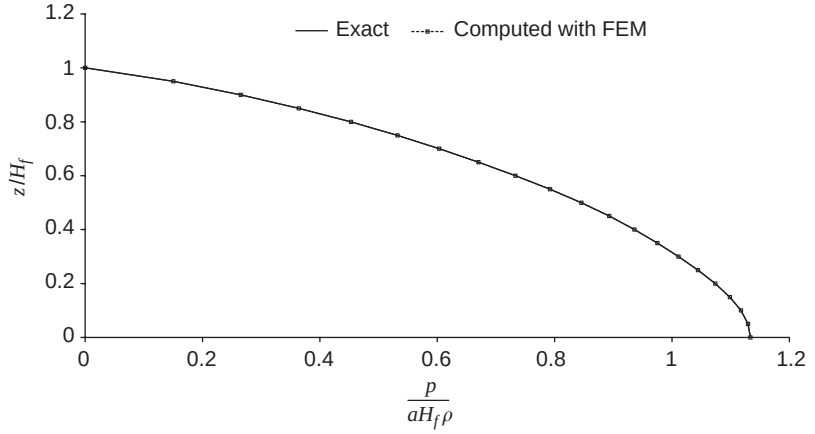

Fig. 5. Peak hydrodynamic pressure distribution on the face of the dam.

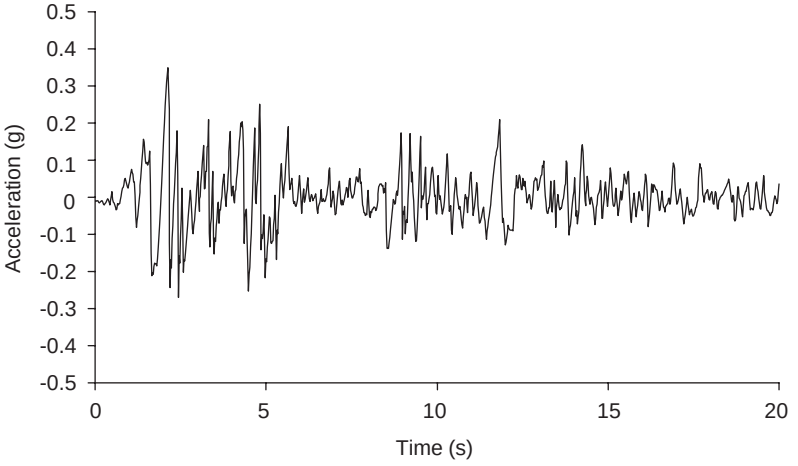

Fig. 6. North–south component of El Centro (1940) ground motion.

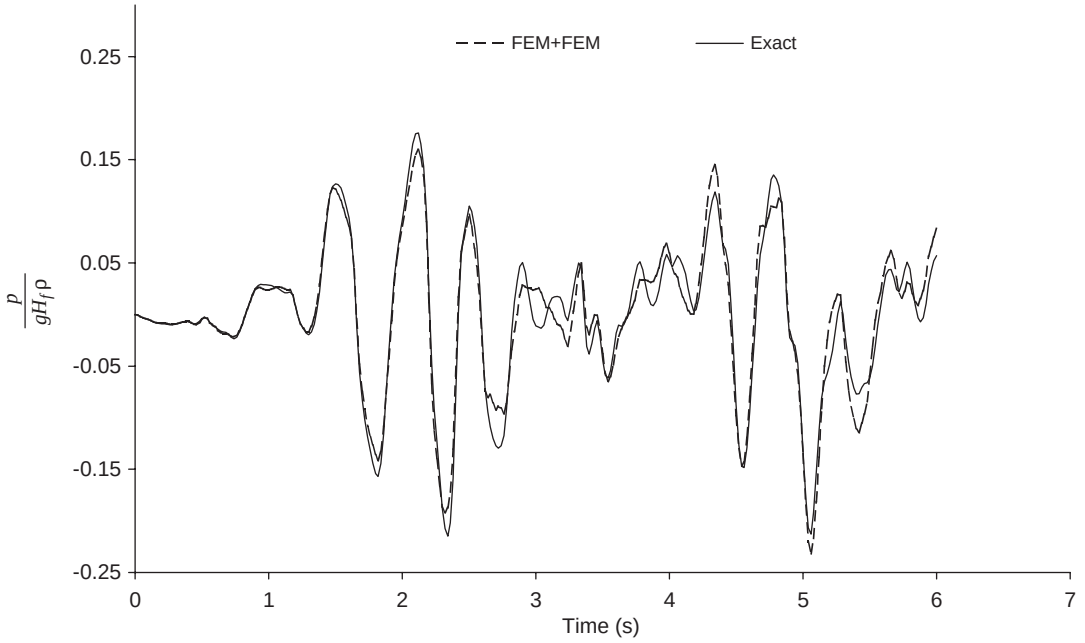

Fig. 7. Comparison of the hydrodynamic pressure at the bottom of the dam.

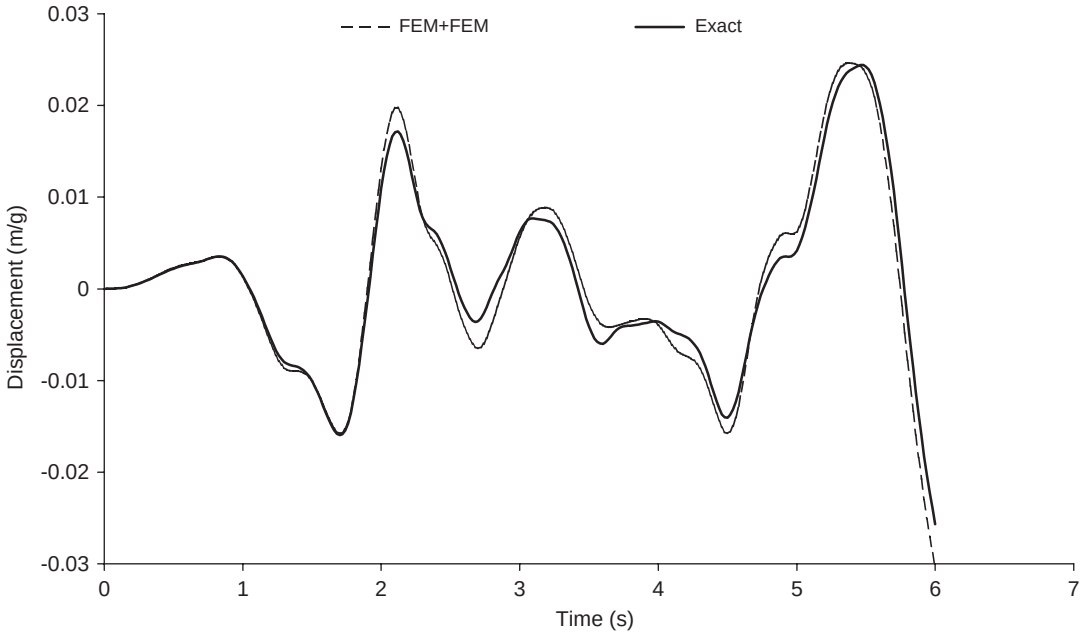

Fig. 8. Displacement at the top of the structure versus time under El Centro ground acceleration.

4.3. Concrete gravity dam

A reservoir of height 180 m, constant along the length of the dam (extending to "infinity") and a width of 15 m (Fig. 9) is analyzed under earthquake ground acceleration (Fig. 6). The same material properties as for the vertical flexible dam are used in this example. The dam bottom is assumed to be rigid, and effects of bottom materials are

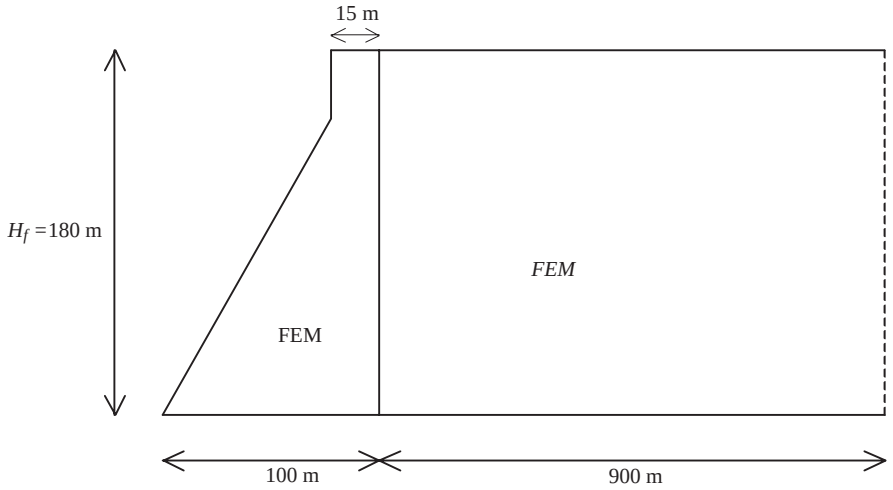

Fig. 9. Concrete gravity dam.

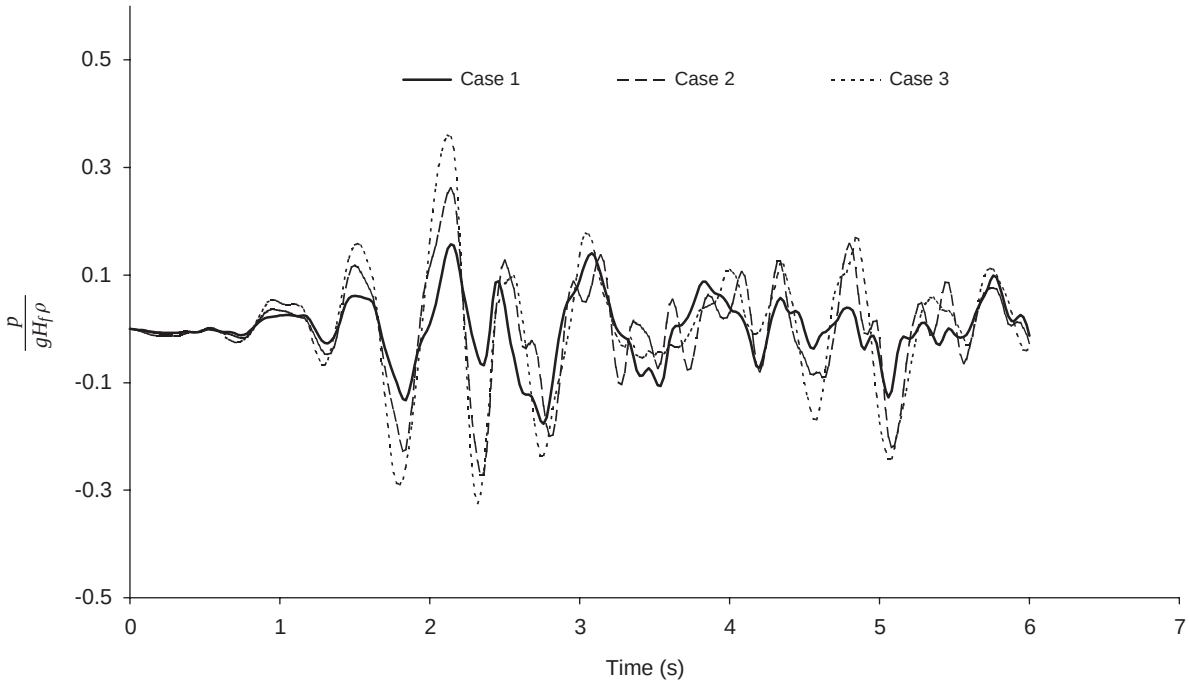

Fig. 10. Hydrodynamic pressure distribution for different wave reflection ratios.

included in the analysis. For the dam structure, 6 elements in the horizontal direction and 12 elements in the vertical direction are used. For the reservoir domain, 40 elements in the horizontal direction and 12 elements in the vertical direction are used. The far end is truncated at a distance of 900 m and Sommerfeld's boundary condition is implemented for the radiating waves. Analyses are performed with a time step of 0.015 s. The hydrodynamic pressure distribution at the bottom and the displacement-time history at the top of the dam are plotted in Figs. 10 and 11, respectively. Since value for α_b from 0 to 1 cover a wide range of materials encountered at the bottom of reservoirs, results are obtained for three different values: $\alpha_b = 0$ (case 1), $\alpha_b = 0.5$ (case 2), and $\alpha_b = 1$ (case3). In Figs. 10 and 11, g is the acceleration due to gravity.

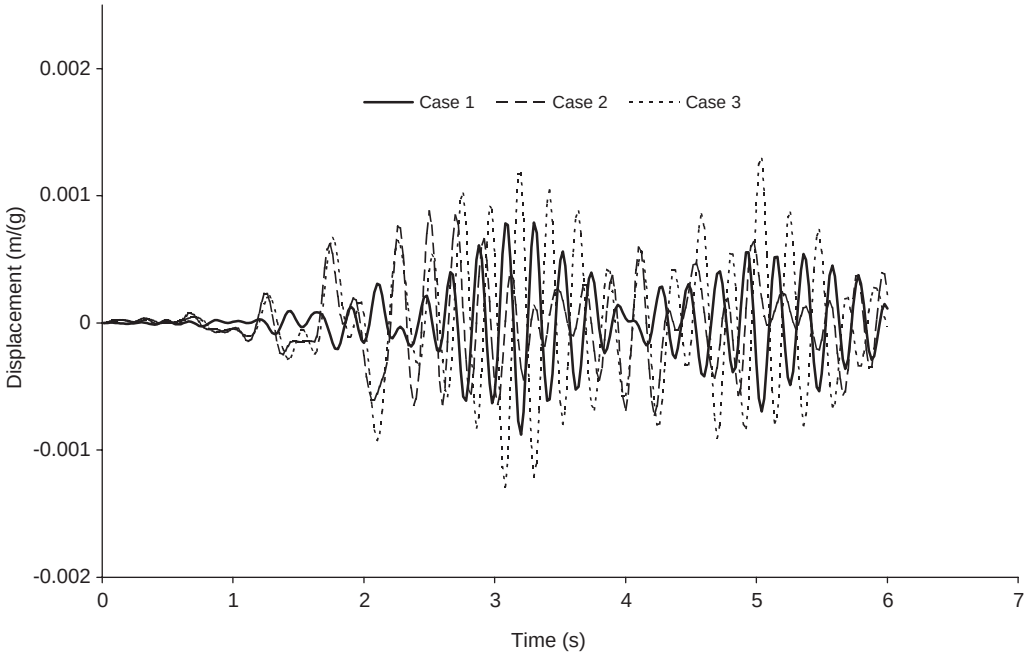

Fig. 11. Displacement at the top of the structure for different wave reflection ratios.

It can be seen from the figures that, an increase of the value of α_b from 0 to 1 results in an increase in the peak value of the displacement and of the hydrodynamic pressure.

5. Conclusions

The dam–reservoir interaction problem in the time domain was studied by coupling the finite element method for the dam and for the reservoir. The effect of the bottom material was also included in the analysis. A substructure technique was used to couple the dam and reservoir equations by using appropriate boundary conditions at the common interfaces. For the truncating boundary at the far end of the reservoir, Sommerfeld's boundary condition was applied. The verification of the proposed method has been successfully realized by the comparisons performed using available results. A final numerical example was carried out to observe the effect of the bottom material on the hydrodynamic pressure distribution and the displacement variation.

Acknowledgements

The authors are thankful to the editor Professor Michael P. Païdoussis and the Associate Editor Professor Shinji Hayama and anonymous reviewers of this paper for their suggestions and comments, which improved the present paper considerably.

References

Bougacha, S., Tassoulas, J.L., 1991. Seismic analysis of gravity dams. Part I: Modeling of sediments. ASCE Journal of Engineering Mechanics 117, 1826–1837.

Cheng, A., 1986. Effect of sediment on earthquake induced reservoir hydrodynamic response. ASCE Journal of Engineering Mechanics 112, 654–664.

Chopra, A.K., 1968. Earthquake behavior of dam–reservoir systems. ASCE Journal of Engineering Mechanics 94, 1475–1499.

Chopra, A.K., Chakrabarti, P., 1981. Earthquake analysis of concrete gravity dams including dam–fluid–foundation rock interaction. Earthquake Engineering and Structural Dynamics 9, 363–383.

Chwang, A.T., Hausner, G.W., 1978. Hydrodynamic pressures on sloping dams during earthquakes, Part 1: Momentum method. Journal of Fluid Mechanics 87, 335–341.

Fenves, G., Chopra, A.K., 1984. Earthquake analysis of concrete gravity dams including bottom absorption and dam–water–foundation rock interaction. Earthquake Engineering and Structural Dynamics 12, 663–683.

Fenves, G., Chopra, A.K., 1985. Effects of reservoir bottom absorption and dam–water–foundation rock interaction on frequency response functions for concrete gravity dams. Earthquake Engineering and Structural Dynamics 13, 13–31.

Ghaemian, M., Ghobarah, A., 1998. Staggered solution schemes for dam–reservoir interaction. Journal of Fluids and Structures 12, 933–948.

Hall, J.F., Chopra, A.K., 1982. Two dimensional dynamic analysis of concrete gravity and embankment dams including hydrodynamic effects. Earthquake Engineering and Structural Dynamics 10, 305–332.

Kuo, J.S.H., 1982. Fluid–structure interactions: Added mass computation for incompressible fluid. UCB/EERC-82/09 Report. University of California, Berkeley, USA.

Lee, G.C., Tsai, C.S., 1991. Time domain analyses of dam–reservoir system Part I: exact solution. ASCE Journal of Engineering Mechanics 117, 1990–2006.

Li, X., Romo, O., Aviles, M.P., 1996. Finite element analysis of dam–reservoir systems using an exact far-boundary condition. Computers and Structures 60, 751–762.

Liu, P.L.F., 1986. Hydrodynamic pressures on rigid dams during earthquakes. Journal of Fluid Mechanics 165, 131–145.

Lotfi, V., Tassoulas, J.L., 1986. Analysis of the response of dams to earthquakes Report GR86-2. The University of Texas, Austin, USA.

Lotfi, V., Roesset, J.M., Tassoulas, J.L., 1987. A technique for the analysis of the response of dams to earthquakes. Earthquake Engineering and Structural Dynamics 15, 463–490.

Maity, D., Bhattacharyya, S.K., 1999. Time domain dynamic analysis of infinite reservoir by finite element method using a novel far-boundary condition. Finite Elements in Analysis and Design 32, 85–96.

Maity, D., Bhattacharyya, S.K., 2003. A parametric study on fluid–structure interaction problems. Journal of Sound and Vibration 263, 917–935.

Medina, F., Dominguez, J., 1989. Boundary elements for the analysis of the seismic response of dams including dam–water–foundation interaction effects. Engineering Analysis 6, 152–157.

Saini, S., Bettess, P., Zienkiewicz, O.C., 1978. Coupled hydrodynamic response of concrete dams using finite and infinite elements. Earthquake Engineering and Structural Dynamics 6, 363–374.

Sharan, S.K., 1987. Time domain analysis of infinite fluid vibration. International Journal for Numerical Methods in Engineering 24, 945–958.

Sommerfeld, A., 1949. Partial Differential Equations in Physics. Academic Press, New York.

Tsai, C.S., Lee, G.C., 1991. Time domain analyses of dam–reservoir system, Part II: Substructure method. ASCE Journal of Engineering Mechanics 117, 2007–2026.

Tsai, C.S., Lee, G.C., Ketter, R.L., 1990. A semi-analytical method for time domain analyses for dam–reservoir interactions. International Journal for Numerical Methods In Engineering 29, 913–933.

Westergaard, H.M., 1933. Water pressure on dams during earthquakes. Transactions of ASCE 98, 418–472.

Yang, C.S., Tsai, C.S., Lee, G.C., 1996. Procedure for time domain seismic analyses of concrete dams. ASCE Journal of Engineering Mechanics 122, 116–122.

Zangar, C.N., Haefei, R.J., 1952. Electric analog indicates effects of horizontal earthquake shock on dams. Civil Engineering 4, 54–55.

Zienkiewicz, O.C., Nath, B., 1963. Earthquake hydrodynamic pressures on arch dams-an electric analogue solution. In: Proceedings of International Civil Engineering Congress, vol. 25, pp. 165-176.